ChemComm

COMMUNICATION

View Article Online
View Journal | View Issue

Cite this: *Chem. Commun.*, 2016, 52, 11292

Received 2nd August 2016,
Accepted 18th August 2016

DOI: 10.1039/c6cc06375f

www.rsc.org/chemcomm

Morphology and phase transformation from $NaCaSiO_3OH$ to $Na_2Ca_2Si_2O_7$ and photoluminescence evolution *via* Eu^{3+}/Tb^{3+} doping†

Mingyue Chen,[a] Zhiguo Xia,*[a] Maxim S. Molokeev[bc] and Qiulin Liu[a]

A facile and controllable ethanol/water aided hydrothermal process was developed to prepare the $NaCaSiO_3OH:Tb^{3+}/Eu^{3+}$ phosphor. The morphologies were *in situ* constructed with the phase transformation from $NaCaSiO_3OH$ to $Na_2Ca_2Si_2O_7$, and the intrinsic crystal structural transformation mechanism and the dependence of their photoluminescence tuning on the Tb^{3+}/Eu^{3+} ratio have been discussed.

The design and synthesis of rare earth (RE) ions doped luminescent materials with controllable morphologies remains a challenge owing to their size/shape-dependent properties and induced potential applications in lighting devices,[1] biological labeling,[2] lasers, displays,[3] *etc.* The physical–chemical properties of materials could be controlled as we desired through a good manipulation of the size and morphology.[4] Therefore, fabrication of RE doped luminescent materials with controlled structures and morphologies is still one of the challenging issues in chemistry and materials science. Amongst them, RE doped silicate materials have been widely investigated due to the versatility in their crystal structures and tunable luminescence properties, which are suitable for application to many fields.[5–8] Usually, high-temperature solid-state reactions are employed to prepare silicate materials. So, the resultant samples appear in aggregation with an irregular shape, and such a preparation method limits the possibility of tuning the morphology and the following properties of the final products. Accordingly, various solution-based preparation techniques, such as co-precipitation,[9] hydrothermal,[10] sol–gel,[11] have been explored to prepare silicate materials with controllable morphologies, which is still a challenge.

Herein, we present a facile pathway toward Eu^{3+}/Tb^{3+}-doped $Na_2Ca_2Si_2O_7$ phosphors that rely on the heat treatment of the $NaCaSiO_3OH:Eu^{3+}/Tb^{3+}$ precursor prepared using a controllable hydrothermal method. By tuning the ethanol/water ($EtOH/H_2O$) ratio, it is possible to yield different precursor morphologies, such as rods, decahedron, distorted octahedron and spindle. Then, we synthesized $Na_2Ca_2Si_2O_7$ with the same particle shapes as those of $NaCaSiO_3OH$, as obtained from the *in situ* construction and phase transformation from $NaCaSiO_3OH$ to $Na_2Ca_2Si_2O_7$. Additionally, the luminescence properties of Eu^{3+}/Tb^{3+} doped $NaCaSiO_3OH$ and $Na_2Ca_2Si_2O_7$ microstructures are comparatively investigated, and the luminescent colors of $Na_2Ca_2Si_2O_7:Tb^{3+},Eu^{3+}$ can be adjusted from red to green depending on the Tb^{3+}/Eu^{3+} ratio, which should be ascribed to the energy transfer of $Tb^{3+} \rightarrow Eu^{3+}$. The work reveals that our current hydrothermal method following a heat treatment process is a facile and efficient way to the synthesis of such phosphors with controlled morphologies.

The preparation method employed for all the presented materials is described in detail in the ESI.† Herein, the X-ray diffraction (XRD) patterns of the $NaCaSiO_3OH$ samples prepared by the addition of different $EtOH/H_2O$ volume ratios are shown in Fig. 1. From Fig. 1 and Fig. S1a (ESI†), it can be observed that all samples exhibit a single phase and all peaks are assigned to the monoclinic phase $NaCaSiO_3OH$ (JCPDS card no. 25-1319). The dependence of the $NaCaSiO_3OH$ morphology on the reaction media of the $EtOH/H_2O$ volume ratio is illustrated well by the scanning electron microscopic (SEM) evaluation of the isolated products (see Fig. 2 and Fig. S1b, c, ESI†). Rod-like particles are obtained when the volume of H_2O is 30 ml (Fig. 2a), and some rods are agglomerated to form rod bunches. From Fig. 2b, the morphology of $NaCaSiO_3OH$ is changing progressively to a nubby shape in the presence of 1 ml EtOH. Increasing the EtOH volume to 5 ml ($EtOH/H_2O$ = 5/25) yields a perfect decahedron shape noted in Fig. 2c, indicating that the decahedral structure may have grown from rods. Based on the high magnification SEM image (the inset of Fig. 2c), the decahedrons with some rips are highly uniform and symmetrical, and they exhibit a bigger size compared to the sample prepared in $EtOH/H_2O$ = 1/29. Upon addition of 10 ml EtOH, the decahedral shape transforms into octahedron one, but the two sides of the selected octahedron are

[a] *School of Materials Sciences and Engineering, University of Science and Technology Beijing, Beijing 100083, China. E-mail: xiazg@ustb.edu.cn; Fax: +86-10-8237-7955; Tel: +86-10-8237-7955*
[b] *Laboratory of Crystal Physics, Kirensky Institute of Physics, SB RAS, Krasnoyarsk 660036, Russia*
[c] *Department of Physics, Far Eastern State Transport University, Khabarovsk, 680021, Russia*

† Electronic supplementary information (ESI) available. See DOI: 10.1039/c6cc06375f

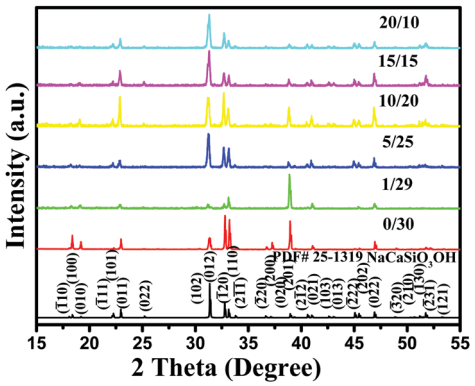

Fig. 1 XRD patterns of $NaCaSiO_3OH$ samples prepared in various volume ratios of EtOH to H_2O. The standard data for $NaCaSiO_3OH$ (JCPDS card no. 25-1319) is shown as a reference.

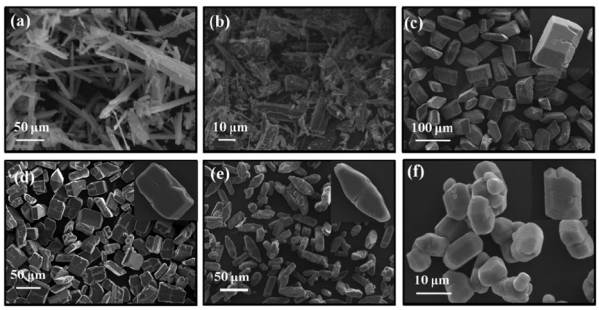

Fig. 2 SEM images of $NaCaSiO_3OH$ samples prepared in different volume ratios of EtOH to H_2O: 0/30 (a), 1/29 (b), 5/25 (c), 10/20 (d), 15/15 (e) and 20/10 (f). The inset images in c–f are the corresponding enlarged single particle.

not smooth (the inset of Fig. 2d). Upon further increasing the EtOH to 15 ml, the spindle shape is developed, and the centre thickness of the spindle is greater than the edge thickness. Then, under a rich amount of EtOH (20–30 ml), pure phase $NaCaSiO_3OH$ is still formed, but the morphology of $NaCaSiO_3OH$ particles become more irregular, even giving rise to crystal aggregates as illustrated in Fig. 2f and Fig. S1b, c (ESI†). More interestingly, it is observed that the higher the EtOH content (5–30 ml), the smaller the particle size. Therefore, we can conclude that the difference of morphologies and sizes in this surfactant/ligand-free system is mainly governed by the amount of the solvent EtOH. Generally, the growth of crystals and the formation of various morphologies are complex processes that are the cooperative results of the inherent structures and the external experimental conditions.[12–14] In our case, two kinds of solvents (H_2O and EtOH) with different polarities and saturated vapour pressures are used as reaction media, producing a distinguished morphology and a size of $NaCaSiO_3OH$. The polarities and saturated vapour pressures of the solvents were found to affect the products under thermal conditions by giving adjustments to the homogenization of the reactants, the amount of individual nucleus formation, the amalgamation and direction preference of growing nucleus.[15] Furthermore, the ratio of two solvents would affect the solubility of the starting materials, the reaction rate and the crystallization rate of products, which result in the various morphologies, as observed in the present and other experiments.

The thermal stability of the $NaCaSiO_3OH$ phase is firstly investigated by thermogravimetric and differential scanning calorimetry (TG-DSC) analysis. From the recorded TG-DSC results during the heat-treatment of $NaCaSiO_3OH$ in air (Fig. 3a), it is apparent that the decomposition starts at 460 °C and finishes at 523 °C with the weight loss of 5.64%, which agrees with the theoretical value (5.76%) calculated from the dehydration of two $NaCaSiO_3OH$ molecules. Hence, the phase decomposition is proposed over the temperature range of 450–530 °C. To verify the occurrence of phase transformation and find the exact phase transformation temperature, variable temperature X-ray diffraction (VT-XRD) is employed *in situ*. As shown in VT-XRD patterns (Fig. 3b), we find that the $NaCaSiO_3OH$ phase is thermally stable up to 450 °C in air. At 500 °C, a mixture of the $NaCaSiO_3OH$ phase and the newly formed $Na_2Ca_2Si_2O_7$ phase (ICSD card no. 95858) appears. However, all the characteristic XRD peaks coincide with the standard pattern of $Na_2Ca_2Si_2O_7$, when the temperature is increased to 600 °C. Even if the heating temperature rises up to 1000 °C continuously, the $Na_2Ca_2Si_2O_7$ phase still maintained, confirming that the temperature of phase transformation from $NaCaSiO_3OH$ to $Na_2Ca_2Si_2O_7$ is about 500 °C, as observed from the TG-DSC results. Fig. 3c shows the SEM images of the resultant $Na_2Ca_2Si_2O_7$. More interestingly, it can be found that the morphologies of $NaCaSiO_3OH$ can be kept *in situ* even if it is sintered at 700 °C to form the $Na_2Ca_2Si_2O_7$ phase. We believe that such a phase transformation synthesis should be a general and facile way to prepare morphology-controllable silicate materials. Moreover, Fig. 3d gives the enlarged image of the individual $Na_2Ca_2Si_2O_7$ particle, and the porous surface character can be observed, which implies the decomposition of $NaCaSiO_3OH$ *via* evaporation of H_2O molecular and the appearance of microscopic pores on the surface of the particles. The intrinsic crystal structural transformation mechanism will also be discussed in the following section.

The phase transformation mechanism for the formation of the $Na_2Ca_2Si_2O_7$ phase with microscopic pores on the particle surface

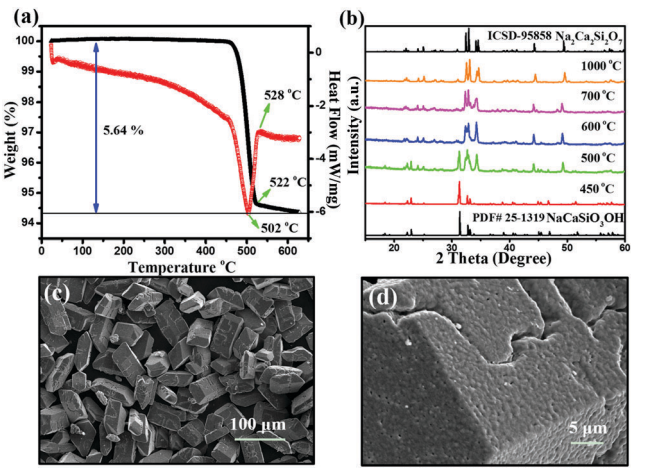

Fig. 3 (a) TG-DSC curves of the as-obtained $NaCaSiO_3OH$, (b) the VT-XRD patterns of $NaCaSiO_3OH$ precursors (EtOH/H_2O = 5/25) by sintering them at different temperatures. (c) SEM images of resultant $Na_2Ca_2Si_2O_7$ when calcining the selected $NaCaSiO_3OH$ *in situ* at 700 °C and (d) the enlarged image of the single $Na_2Ca_2Si_2O_7$ particle.

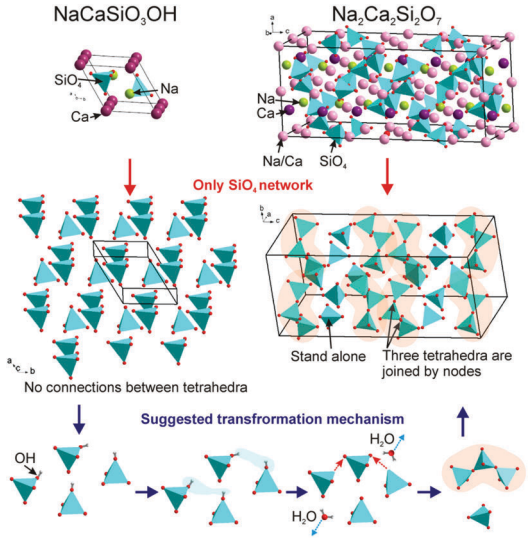

Fig. 4 The comparative description of the crystal structures of $NaCaSiO_3OH$ and $Na_2Ca_2Si_2O_7$, and the transformation mechanism from $NaCaSiO_3OH$ to $Na_2Ca_2Si_2O_7$.

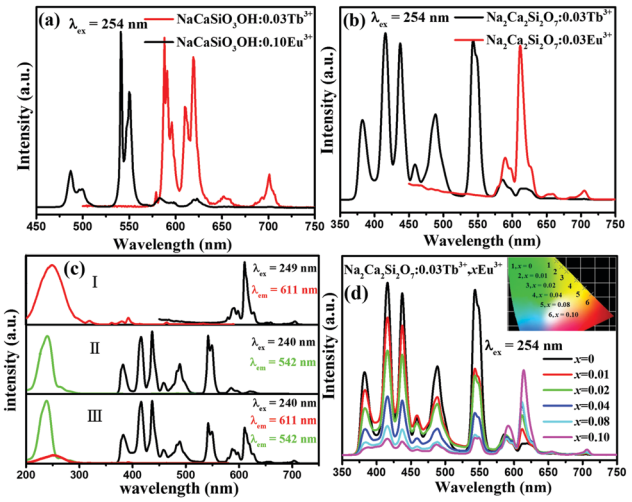

Fig. 5 PL spectra $NaCaSiO_3OH$:0.10Eu^{3+}/0.03Tb^{3+} (a) and $Na_2Ca_2Si_2O_7$:0.10Eu^{3+}/0.03Tb^{3+} (b) phosphors. PLE and PL spectra of $Na_2Ca_2Si_2O_7$:0.03Eu^{3+} (c) -I, $Na_2Ca_2Si_2O_7$:0.03Tb^{3+} (c) -II, and $Na_2Ca_2Si_2O_7$:0.03Tb^{3+}, 0.03Eu^{3+} (c) -III phosphors. (d) PL spectra of $Na_2Ca_2Si_2O_7$:0.03Tb^{3+},xEu^{3+} phosphors with different Eu^{3+} doped concentrations (*x*), the inset shows the corresponding CIE chromaticity diagram.

is proposed in Fig. 4. As we know, both the $NaCaSiO_3OH$ and $Na_2Ca_2Si_2O_7$ belong to monoclinic phases, but their space groups are $P2_1/m$ and $C2/c$ respectively and their cell parameters are absolutely distinguished. Therefore, such a phase transformation doesn't belong to the topotactic transformation because two structures have unit cells without relations. Besides these, other differences of the two structures are manifested as follows: (1) $Na_2Ca_2Si_2O_7$ consists of Ca, Na/Ca, Na and Si sites, but $NaCaSiO_3OH$ merely consists of Ca, Na and Si cations, no Ca/Na mixing exists in $NaCaSiO_3OH$; (2) networks of SiO_4 polyhedra are different, namely, there are isolated SiO_4 in $NaCaSiO_3OH$ and two isolated groups (SiO_4 and Si_3O_{10}) in $Na_2Ca_2Si_2O_7$ (see Fig. 4). However, the phase relations between $NaCaSiO_3OH$ and $Na_2Ca_2Si_2O_7$ should be considered. In this case we can suggest that OH groups of two SiO_3OH tetrahedra combine with two H ions from other two SiO_3OH tetrahedra forming two H_2O molecules. The remaining two SiO_3 and two SiO_4 form Si_3O_{10} + SiO_4 as illustrated in the bottom panel of Fig. 4. The possible chemical reaction equation of the formation of $Na_2Ca_2Si_2O_7$ from $NaCaSiO_3OH$ could be described as follows:

$$NaCaSiO_3OH + NaCaSiO_3OH \xrightarrow[700\,^\circ C]{\text{in air}} Na_2Ca_2Si_2O_7 + H_2O$$

In the phase transition process, the dehydration from $NaCaSiO_3OH$ results in the generation of H_2O; then, a large amount of vacancies should be formed during the formation of the new $Na_2Ca_2Si_2O_7$ phase. The expansion of vacancies may lead to the formation of cracks and microscopic pores at the $Na_2Ca_2Si_2O_7$ polyhedron facets. The SEM images of calcined product $Na_2Ca_2Si_2O_7$ (Fig. 3d) show that the polyhedrons possess many microscopic holes, which supports the above proposed mechanism.

Our experiments have also shown that both $NaCaSiO_3OH$ and $Na_2Ca_2Si_2O_7$ are good hosts for the luminescent materials formed *via* the Eu^{3+}/Tb^{3+} doping. It should be mentioned that the doping of Eu^{3+}/Tb^{3+} into $NaCaSiO_3OH$ and $Na_2Ca_2Si_2O_7$ does not change the phase purity and morphology of the final products as displayed in Fig. S3 (ESI†). Herein, the luminescence properties of Eu^{3+} and Tb^{3+} singly or/and codoped $NaCaSiO_3OH$ and $Na_2Ca_2Si_2O_7$ samples with a decahedron-like shape ($EtOH/H_2O$ = 5/25) were comparatively investigated. Fig. 5a and b show the photoluminescence (PL) emission spectra of $NaCaSiO_3OH$:0.10Eu^{3+}/0.03Tb^{3+} and $Na_2Ca_2Si_2O_7$:0.10Eu^{3+}/0.03Tb^{3+} samples, respectively. $NaCaSiO_3OH$:Eu^{3+} shows a strong red luminescence originating from the $^5D_0 \rightarrow {}^7F_J$ (J = 0, 1, 2, 3, 4) transitions of Eu^{3+} ions under 254 nm excitation.[16,17] For the $Na_2Ca_2Si_2O_7$:Eu^{3+} sample, the PL spectrum exclusively contains the characteristic emission of Eu^{3+} cantered at 611 nm. On the other hand, $NaCaSiO_3OH$:Tb^{3+} shows a series of strong green emission lines with a maximum at about 542 nm, which are all ascribed to $^5D_4$–^7F_J (J = 6, 5, 4, 3) transitions of Tb^{3+} corresponding to $^5D_4$–$^7F_6$ (488 nm), $^5D_4$–$^7F_5$ (542 and 550 nm), $^5D_4$–$^7F_4$ (583 nm) and $^5D_4$–$^7F_3$ (625 nm), respectively, which are similar to other Tb^{3+}-containing phosphors, such as $Tb_2(MoO_4)_3$.[18,19] For the $Na_2Ca_2Si_2O_7$:Tb^{3+}, the emission spectral lines in the blue region are found to be at 416 nm ($^5D_3$–$^7F_5$) and 437 nm ($^5D_3$–$^7F_4$) with high emission intensity. However, they do not emerge in the emission spectra of $NaCaSiO_3OH$:Tb^{3+}, which means that there is a relatively low photon energy of $Na_2Ca_2Si_2O_7$ compared to that of $NaCaSiO_3OH$. Moreover, the intensity ratio of $^5D_0 \rightarrow {}^7F_2$ and $^5D_0 \rightarrow {}^7F_1$ transitions of Eu^{3+} ions in different hosts is related to the activator symmetry occupied in the lattice. The strong emission from $^5D_0 \rightarrow {}^7F_2$ compared to that of $^5D_0 \rightarrow {}^7F_1$ in $Na_2Ca_2Si_2O_7$:0.10Eu^{3+} denotes that there is relatively low symmetry for $Na_2Ca_2Si_2O_7$. Therefore, it is found that there is obvious difference in the emission spectra of $NaCaSiO_3OH$:Eu^{3+} and $Na_2Ca_2Si_2O_7$:Eu^{3+}; as well as $NaCaSiO_3OH$:Tb^{3+} and $Na_2Ca_2Si_2O_7$:Tb^{3+}. The effects can be attributed to the different coordination environments and symmetry around the Tb^{3+}/Eu^{3+} ions in the $NaCaSiO_3OH$ and

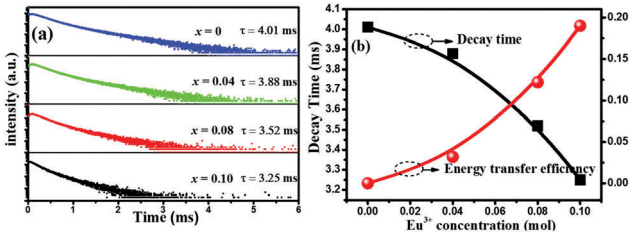

Fig. 6 (a) The decay curves and lifetime values of Tb^{3+} in $Na_2Ca_2Si_2O_7$: $0.03Tb^{3+}$,xEu^{3+} with different Eu^{3+} contents (x): x = 0, 0.04, 0.08 and 0.10. (b) Dependence of the fluorescence lifetime of the Tb^{3+} and energy transfer efficiency on doped Eu^{3+} molar concentration in $Na_2Ca_2Si_2O_7$: $0.03Tb^{3+}$,xEu^{3+} samples.

$Na_2Ca_2Si_2O_7$ hosts.[12] Furthermore, from Fig. 5c, the spectral overlap between the PL spectrum of $Na_2Ca_2Si_2O_7$:Tb^{3+} and photoluminescence excitation (PLE) spectrum of $Na_2Ca_2Si_2O_7$:Eu^{3+} can be observed, and the PL spectra of $Na_2Ca_2Si_2O_7$:Tb^{3+},Eu^{3+} consist of the peaks at 611 nm and 542 nm attributed to Eu^{3+} and Tb^{3+}, respectively. The results suggest that the energy transfer can occur from Tb^{3+} to Eu^{3+},[20] and the emitting colour can be tuned from green to yellow and red *via* energy transfer of $Tb^{3+} \rightarrow Eu^{3+}$ by tuning the doped Eu^{3+} concentrations as shown in Fig. 5d and the inset.

In order to further investigate the energy transfer process between Tb^{3+} and Eu^{3+}, the decay curves of Tb^{3+} by monitoring the emission transition at 542 nm were measured and depicted in Fig. 6(a). The decay curve can be well fitted with a second-order exponential decay mode by using eqn (1):[21–23]

$$I(t) = A_1 \exp(-t/\tau_1) + A_2 \exp(-t/\tau_2) \quad (1)$$

where I is the luminescence intensity, A_1 and A_2 are constants, t is the time, τ_1 and τ_2 are rapid and slow lifetime values for exponential components, respectively. Based on the eqn (1), one can obtain the A_1, A, τ_1 and τ_2 values by fitting of the decay curves. Therefore, the effective lifetime constant (τ^*) can be calculated as eqn (2):

$$\tau^* = (A_1\tau_1^2 + A_2\tau_2^2)/(A_1\tau_1 + A_2\tau_2) \quad (2)$$

The effective decay time (τ^*) was calculated to be 4.01, 3.88, 3.52 and 3.25 ms for $Na_2Ca_2Si_2O_7$:$0.03Tb^{3+}$,xEu^{3+} with x = 0, 0.04, 0.08 and 0.10, respectively. The energy-transfer efficiency (η_T) from Tb^{3+} to Eu^{3+} ions can be expressed as the following eqn (3):[23–26]

$$\eta_T = 1 - (I_S/I_{S_0}) = 1 - (\tau_S/\tau_{S_0}) \quad (3)$$

where τ_{S_0} and τ_S stand for the lifetimes of Tb^{3+} in the absence and the presence of Eu^{3+} respectively. With the increase in the Eu^{3+} concentration, the η_T value is calculated and the results are shown in Fig. 6(b). As displayed in Fig. 6(b), the average lifetime decreased monotonically and the energy-transfer efficiency increased with the increasing Eu^{3+} content. The η_T value reached a maximum of 19% at x = 0.10.

In summary, we have presented for the first time a simple hydrothermal method for the synthesis of highly crystallized $NaCaSiO_3OH$ particles with a controlled morphology/size in the presence of EtOH as both the solvent and the structure-directing agent. More importantly, the as-prepared $NaCaSiO_3OH$ can be *in situ* transferred into $Na_2Ca_2Si_2O_7$ by the heat-treatment in air, and the morphologies of the as-prepared $NaCaSiO_3OH$ have been kept without any agglomerations. In principle, this method offers a new alternative strategy to generate silicate materials. Moreover, when $Na_2Ca_2Si_2O_7$ is codoped with Eu^{3+} and Tb^{3+} with an appropriate ratio, the emission colours of the $Na_2Ca_2Si_2O_7$: Tb^{3+},Eu^{3+} phosphors can be tuned from green to yellow and red. It is expected that the morphology-controlled $Na_2Ca_2Si_2O_7$: Tb^{3+},Eu^{3+} micro-particles will provide potential applications for micro/nano functional devices.

The present work was supported by the National Natural Science Foundation of China (Grant No. 51572023 and 51272242), the Fundamental Research Funds for the Central Universities (FRF-TP-15-003A2) and the Russian Foundation for Basic Research (Grant No. 15-52-53080 GFEN_a).

Notes and references

1 S. Sivakumar, F. C. J. M. van Veggel and M. Raudsepp, *J. Am. Chem. Soc.*, 2005, **127**, 12464.
2 G. S. Yi, H. C. Lu, S. Y. Zhao, G. Yue, W. J. Yang, D. P. Chen and L. H. Guo, *Nano Lett.*, 2004, **4**, 2191.
3 *Phosphor Handbook*, ed. S. Shionoya and W. M. Yen, CRC Press, Boca Raton, FL, 1999.
4 C. Burda, X. Chen, R. Narayanan and M. A. El-Sayed, *Chem. Rev.*, 2005, **105**, 1025.
5 W.-W. Maria, M. Göckeritz, K. Uwe, L. Christoph and G. Gerald, *Eur. J. Inorg. Chem.*, 2015, 2426.
6 Y. Wei, C. C. Lin, Z. W. Quan, M. S. Molokeev, V. V. Atuchin, T. S. Chan, Y. J. Liang, J. Lin and G. G. Li, *RSC Adv.*, 2016, **6**, 57261.
7 H. P. Ji, L. Wang, M. S. Molokeev, N. Hirosaki, R. J. Xie, Z. H. Huang, Z. G. Xia, O. M. Ten Kate, L. H. Liu and V. V. Atuchin, *J. Mater. Chem. C*, 2016, **4**, 6855.
8 Z. G. Xia, Y. Y. Zhang, M. S. Molokeev, V. V. Atuchin and Y. Luo, *Sci. Rep.*, 2013, **3**, 3310.
9 J. S. Lee and Y. J. Kim, *J. Nanosci. Nanotechnol.*, 2013, **13**, 3685.
10 D. Ananias, F. A. A. Paz, D. S. Yufit, L. D. Carlos and J. Rochã, *J. Am. Chem. Soc.*, 2015, **137**, 3051.
11 R. Chrysafi, T. Perraki and G. Kakali, *J. Eur. Ceram. Soc.*, 2007, **27**, 1707.
12 G. G. Li, C. Peng, C. M. Zhang, Z. H. Xu, M. M. Shang, D. M. Yang, X. J. Kang, W. X. Wang, C. X. Li, Z. Y. Cheng and J. Lin, *Inorg. Chem.*, 2010, **49**, 10522.
13 C. V. Ramana, V. V. Atuchin, I. B. Troitskaia, S. A. Gromilov, V. G. Kostrovsky and G. B. Saupe, *Solid State Commun.*, 2009, **149**, 6.
14 V. V. Atuchin, T. A. Gavrilova, S. A. Gromilov, V. G. Kostrovsky, L. D. Pokrovsky, I. B. Troitskaia, R. S. Vemuri, G. C. Franco and C. V. Ramana, *Cryst. Growth Des.*, 2009, **9**, 1829.
15 J. Zhang, L. D. Sun, J. L. Yin, H. L. Su, C. S. Liao and C. H. Yan, *Chem. Mater.*, 2002, **14**, 4172.
16 G. Jia, M. Yang, Y. H. Song, H. P. You and H. J. Zhang, *Cryst. Growth Des.*, 2009, **9**, 301.
17 V. V. Atuchin, A. S. Aleksandrovsky, O. D. Chimitova, T. A. Gavrilova, A. S. Krylov, M. S. Molokeev, A. S. Oreshonkov, B. G. Bazarov and J. G. Bazarova, *J. Phys. Chem. C*, 2014, **118**, 15404.
18 Z. H. Xu, C. X. Li, G. G. Li, R. T. Chai, C. Peng, D. Y. Yang and J. Lin, *J. Phys. Chem. C*, 2010, **114**, 2573.
19 V. V. Atuchin, A. S. Aleksandrovsky, O. D. Chimitova, A. S. Krylov, M. S. Molokeev, B. G. Bazarov, J. G. Bazarova and Z. G. Xia, *Opt. Mater.*, 2014, **36**, 1631.
20 J. Zhou and Z. G. Xia, *J. Mater. Chem. C*, 2014, **2**, 6978.
21 C. H. Huang, T. M. Chen, W. R. Liu, Y. C. Chiu, Y. T. Yeh and S. M. Jang, *ACS Appl. Mater. Interfaces*, 2010, **2**, 259.
22 C. H. Huang and T. M. Chen, *J. Phys. Chem. C*, 2011, **115**, 2349.
23 G. Li, Y. Zhang, D. Geng, M. Shang, C. Peng, Z. Cheng and J. Lin, *ACS Appl. Mater. Interfaces*, 2012, **4**, 296.
24 W. J. Yang and T. M. Chen, *Appl. Phys. Lett.*, 2006, **88**, 101903.
25 K. H. Kwon, W. B. Im, H. S. Jang, H. S. Yoo and D. Y. Jeon, *Inorg. Chem.*, 2009, **48**, 11525.
26 P. I. Paulose, G. Jose, V. Thomas, N. V. Unnikrishnan and M. K. R. Warrier, *J. Phys. Chem. Solids*, 2003, **64**, 841.